Bulletin of the Seismological Society of America, 89, 5, pp. 1395–1400, October 1999

Iterative Deconvolution and Receiver-Function Estimation

by Juan Pablo Ligorría and Charles J. Ammon

Abstract We describe and apply an iterative, time-domain deconvolution approach to receiver-function estimation and illustrate the reliability and advantages of the technique using synthetic- and observation-based examples. The iterative technique is commonly used in earthquake time-function studies and offers several advantages in receiver-function analysis such as intuitively stripping the largest receiver-function arrivals from the observed seismograms first and then the details; long-period stability by *a priori* constructing the deconvolution as a sum of Gaussian pulses; and easy generalization to allow multiwaveform deconvolution for a single receiver-function estimate.

Introduction

Receiver-function analysis (e.g., Langston, 1979) is a straightforward, simple method of extracting constraints on crust and upper-mantle structure from teleseismic waveforms recorded at three-component seismic stations. A receiver function is the time series that when convolved with the vertical-component seismogram reproduces the horizontal-component seismogram, and the timing and amplitude of the arrivals in the receiver function are sensitive to the local earth structure (Langston, 1979). Langston (1979) pointed out that the basic characteristic of receiver functions, perhaps most impressive is the clean, causal, seismogram-like signal that results from the deconvolution of the vertical from the radial response of a plane-layered structure. The simplicity of the method assures that it is a routine component of analyzing observations from permanent network stations and portable stations deployed as part of passive-source temporary networks, and the wide application of the technique has produced several complete descriptions of the receiver-function methodology (e.g., Langston, 1979; Owens, 1984; Ammon *et al.,* 1990; Ammon 1991; Cassidy, 1992; Mangino *et al.,* 1993).

Computing a receiver function is a deconvolution problem, and we refer the reader to Oldenburg (1981) for a comprehensive discussion of deconvolution methods. The most commonly employed method in receiver-function studies is a water-level-stabilized, frequency-domain division (e.g., Clayton and Wiggins, 1976), although others have used time-domain approaches (e.g., Gurrola *et al.,* 1995; Sheehan *et al.,* 1995) based on the linear inverse theory. When the data are wideband with good signal-to-noise levels, most deconvolution methods work well, and the advantages of one technique over the other are insignificant. Thus, often the best approach to compute receiver functions for permanent stations with years of data available is simply to exploit signals from large events. However, for select azimuths at most permanent stations and in the case of most temporary deployments, we never have enough observations from all azimuths, and we must incorporate signals from smaller events, which leads to difficult deconvolutions and noisy receiver functions. Then the choice of a deconvolution technique may make a difference. No deconvolution approach outperforms all others in all instances, and in difficult cases, it is best to apply different approaches to try to extract the best results from the observations.

In this note, we add another tool to the receiver-function toolbox and describe our use of an iterative time-domain deconvolution commonly used to estimate large-earthquake source time functions (Kikuchi and Kanamori, 1982). The iterative time-domain approach has several desirable qualities such as a constraint on the spectral shape at long periods that can be advantageous in receiver-function analyses and an intuitive stripping of information from the original signal, garnering the largest, most important features first, and then extracting the details. The mathematical basis of the approach is clearly described in Kikuchi and Kanamori (1982), so we focus this note on examples.

Receiver-Function Iterative Deconvolution

In receiver-function estimation, the foundation of the iterative deconvolution approach is a least-squares minimization of the difference between the observed horizontal seismogram and a predicted signal generated by the convolution of an iteratively updated spike train with the vertical-component seismogram. For this discussion, we will assume that we are estimating the radial receiver function, but the approach is equally applicable to the transverse motion and can be easily generalized to accommodate simultaneous deconvolution of any number of signals. First, the vertical component is cross-correlated with the radial component to estimate the lag of the first and largest spike in the receiver function (the optimal time is that of the largest peak

in the absolute sense in the cross-correlation signal). The spike amplitude is estimated by solving a simple equation listed in Kikuchi and Kanamori (1982). Then the convolution of the current estimate of the receiver function with the vertical-component seismogram is subtracted from the radial-component seismogram, and the procedure is repeated to estimate other spike lags and amplitudes. With each additional spike in the receiver function, the misfit between the vertical and receiver-function convolution and the radial-component seismogram is reduced, and the iteration halts when the reduction in misfit with additional spikes becomes insignificant.

Our goal is not to present a solution to all receiver-function estimation problems nor to claim that the iterative approach can outperform other methods in every instance. Instead, our purpose is to describe a new tool suitable for application in receiver-function analyses. We introduce the iterative time-domain approach using several numerical examples and then conclude with examples that include short-period and broadband observations.

Numerical Experiments

We begin with two simple layer-over-a-half-space models, one with a sharp boundary and one with a smooth transition from a crustlike layer to a mantle-like half-space. Our third example is constructed using a more complex velocity model based on the refraction wide-angle reflection results of Benz *et al.* (1990). In each case, the synthetic seismograms were computed using the method of Randall (1989), which is based on the reflection-matrix technique of Kennett (1983). The seismograms were computed to correspond to a compressional wave arriving with a horizontal slowness of 0.06 sec/km, equivalent to a shallow source about 60° distant. The results shown in Figures 1 and 2 include a comparison of the iterative time domain with a water-level receiver-function estimate. In each case, we present the receiver functions computed using Gaussian width factors of 1.5 and 2.5. The Gaussian width factor controls the bandwidth of the signal; the larger the value, the larger the bandwidth (2.5 is a value commonly used in receiver-function analyses). Also, in each case, we allowed iteration to continue until the change in fit resulting from the addition of a spike was 0.01%.

For the sharp contrast model (Fig. 1), each significant arrival is accurately recovered; for the smooth-transition model, the response is recovered well, but not perfectly. Although noticeable in the time-domain signals, the differences in the receiver-function estimates are limited to the frequencies above approximately 1 Hz and are a result of the Gaussian filter width we selected for the process. Such details are inaccessible with even a modest amount seismic noise ubiquitous in observed seismograms, so these minor differences pose no problem for analysis.

In Figure 2, we compare the iterative time-domain and frequency-domain approaches for a more complex velocity

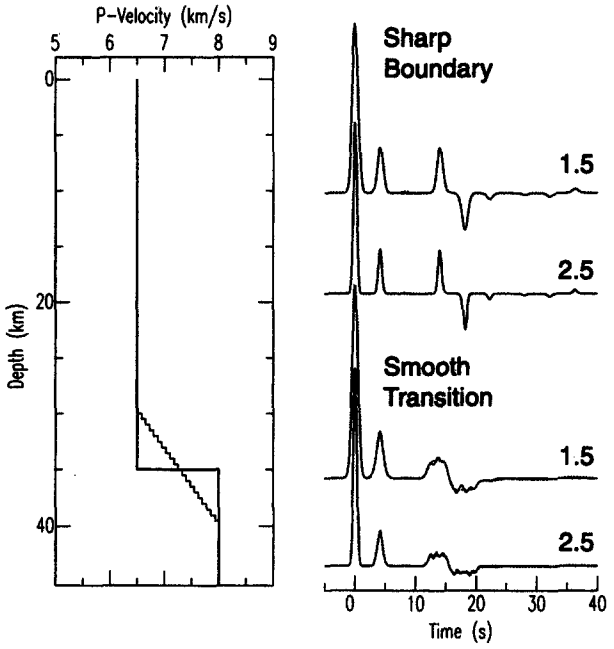

Figure 1. Comparison of frequency-domain (water-level) and iterative time-domain deconvolution results for two receiver responses with contrasting frequency characteristics. The estimated receiver functions are plotted on top of each other for two Gaussian pulse widths (shown above the right edge of the signals) for each model.

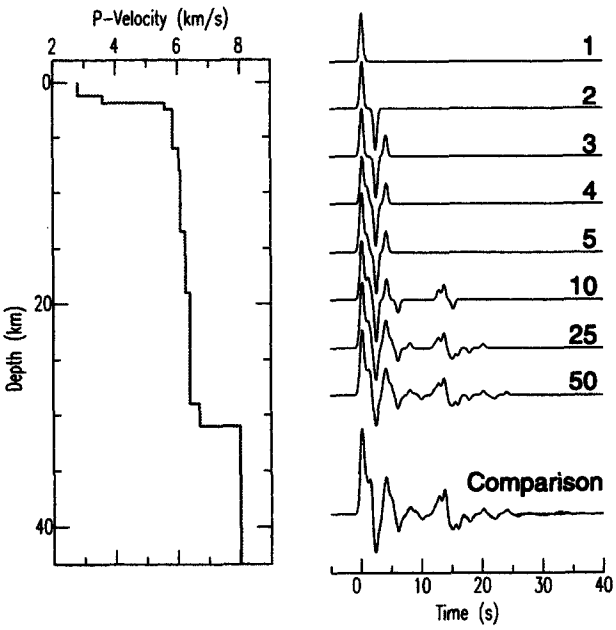

Figure 2. Comparison of the frequency-domain and time-domain receiver-function estimates for a more complicated velocity model. The intermediate estimates of the receiver function for select iterations are shown on the upper right. The receiver function that explains 95.5% of the original signal power in the radial response is compared with the frequency-domain solution on the lower right.

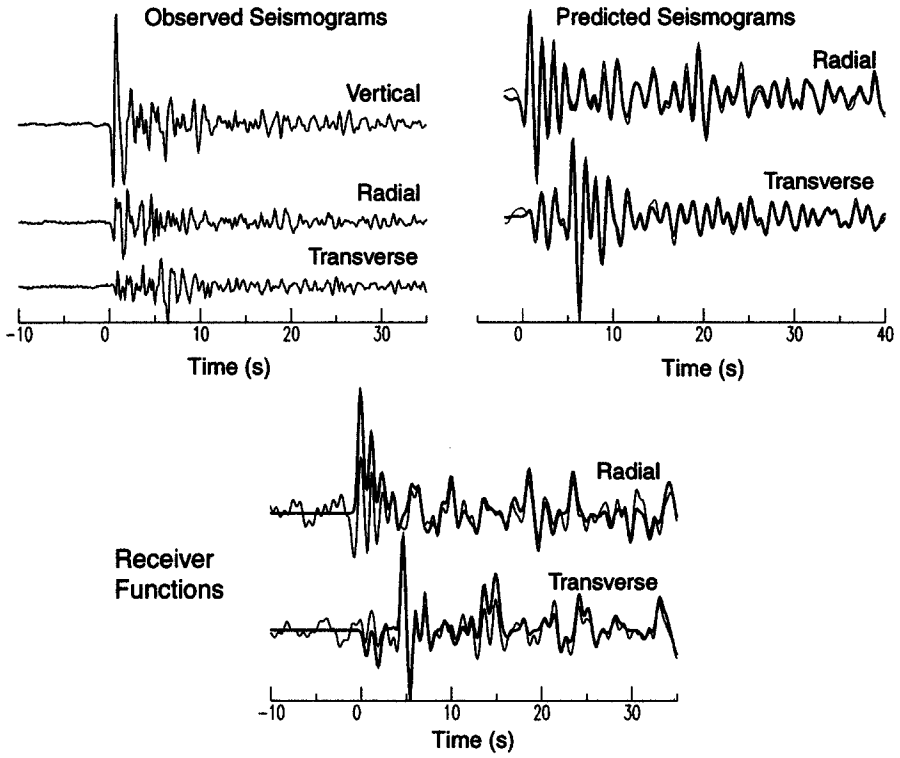

Figure 3. Receiver-function estimation using a short-period signal from the 1988 to 1989 PASSCAL Basin and Range experiment. The original signals from a 500-km-deep, mb 5.2 earthquake are shown in the upper left; the receiver functions estimated using a water-level frequency-domain approach are compared with those of the iterative time-domain approach in the lower panel. The predicted horizontal signals (the iterative deconvolution convolved with the observed vertical) are compared with the observed horizontal signals in the upper-right panel.

structure. The variation of velocity with depth is shown on the left, and the iterative construction of the radial receiver-function estimate is shown on the right (the numbers to the right of each signal refer to the number of spikes in the receiver-function estimate). Receiver functions estimated from iterative time- and frequency-domain approaches are overlaid on the lower right. The iterative time-domain receiver function shown satisfies the convolution definition of a receiver function (convolve the radial receiver function and the vertical seismogram to match the radial seismogram) to within 0.5% of the signal power. The comparison is excellent, although the match late (greater than 30 sec) in the receiver function is less accurate because we limited the number of spikes recovered by the iterative process. We can match the frequency-domain result at later lag times, but we chose to include only enough spikes to match all the important arrivals.

Applications to Noisy Observations

We illustrate the advantages of the iterative time-domain technique with observed seismograms and begin with an example using signals recorded during the 1988 PASSCAL Basin and Range Passive Source experiment. These data include intermediate and short-period signals and like all deployments have their share of noisy data. Several authors have used these data to investigate the velocity structure beneath the region (e.g., Owens and Randall, 1990; McNamara and Owens, 1993; Randall and Owens, 1994; Peng and Humphreys, 1997), and we refer readers to their works for detailed locations, instrument descriptions, and interpretation of the receiver functions. For an illustration of the potential of short-period observations in receiver-function analysis, we refer the reader to Julia *et al.* (1998).

In Figure 3, we present the results of a receiver-function estimation using a short-period station located near the center of the PASSCAL temporary network. The teleseismic *P* wave was generated by an mb 5.3, 500-km-deep earthquake, located about 82° to the southwest of the seismometers. In Figure 3, the recorded seismograms are shown in the upper left, the radial and transverse receiver functions estimated using water-level and iterative time-domain approaches are overlaid in the lower panel, and the predicted radial and transverse seismograms (the match from the water-level deconvolutions is similar) are presented in the upper right. The predictions are quite good, fitting about 95% of the observed power in the horizontal seismograms. The agreement in receiver-function estimates is also good, most arrivals are visi-

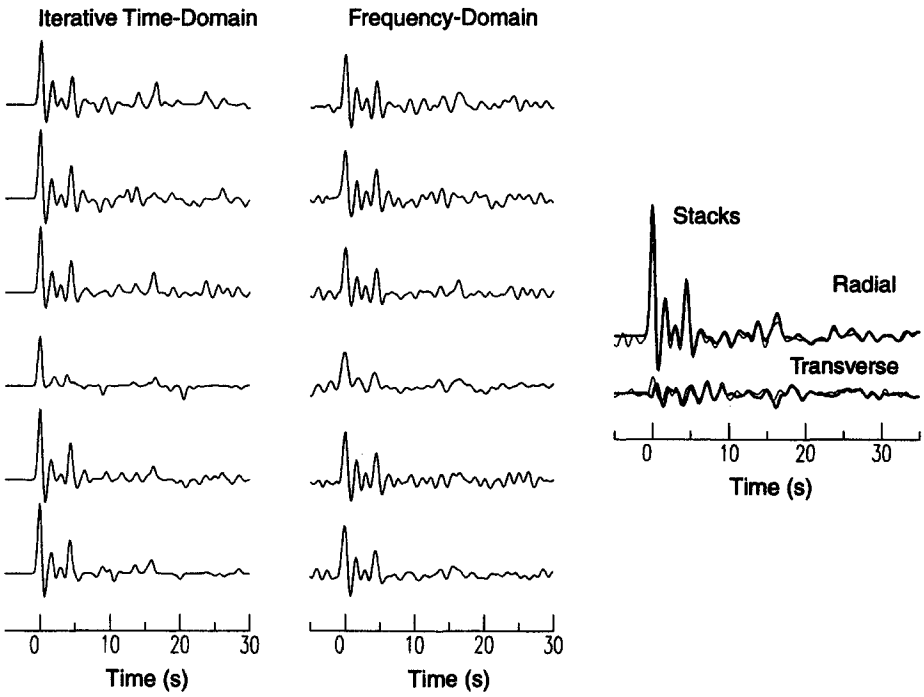

Figure 4. Comparison of receiver-function deconvolutions for events approaching station ANMO, Albuquerque, New Mexico, from the southeast. On the left are the time-domain estimates of the radial receiver function, in the middle are the corresponding water-level frequency-domain receiver functions, and on the right are the average radial and transverse receiver functions from these six events (the thick line identifies the time-domain estimate).

ble on each receiver function. However, the long-period stability of the iterative time-domain results is evident in the amplitude of the early arrivals. Unlike the water-level deconvolution, the time-domain signals have flat spectral levels at long periods (by design because the results are a sum of Gaussian pulses, and all reasonable receiver responses are relatively flat at long periods), and the estimated receiver function does not suffer the acausal trough surrounding the *P* arrival that decreases the amplitude of the first few arrivals on the water-level radial receiver function. Also, the noise running throughout both the radial and transverse frequency-domain receiver functions is absent in the time-domain results.

Next, we illustrate the approach on relatively simple and relatively complex receiver functions from two broadband seismic stations, ANMO, located near Albuquerque, New Mexico, and MLA, located near Mammoth Lakes, California. Based on an examination of the observed receiver functions, the crustal structure to the southeast of ANMO is relatively simple, and a comparison of time- and frequency-domain receiver-function estimates is presented in Figure 4. On the left and center of the figure are individual receiver functions estimated using the two approaches. For these well-behaved signals, the results are similar, but the sometimes inescapable limitations of deconvolution are evident for both methods on the fourth deconvolution from the top. Neither technique produces a satisfactory result on this waveform. On the right, we show the averages of the frequency-domain and iterative time-domain receiver functions (excluding the problematic signal). The results compare very well and differ primarily in the amplitude of the *P* arrival, which is related to increased bandwidth in the iterative time domain. Examination of the spectra of the individual estimates indicates that the iterative time-domain approach produces more coherent amplitude spectra than the water-level approach, but on the average, time-domain variability between the two methods is small.

The receiver responses at MLA are much more complex as a result of its location in the Long Valley Caldera, a structure with a shallow low-velocity layer with a large velocity contrast at its base. The results are presented in Figure 5 using the same format as Figure 4. The complexity of the receiver response is apparent in the receiver functions estimated with either approach, and the results from both techniques vary from waveform to waveform.

Each signal begins with a small arrival (i.e., the *P* wave) and is followed by a large *P*-to-*S* converted phase from the bottom of the surface layer. That *P* arrival actually has an amplitude similar to that observed at ANMO, but it is overwhelmed by the converted phase and reverberations in the caldera fill. Note how consistent the *P* arrival is on the iterative time-domain estimates but indistinguishable from the

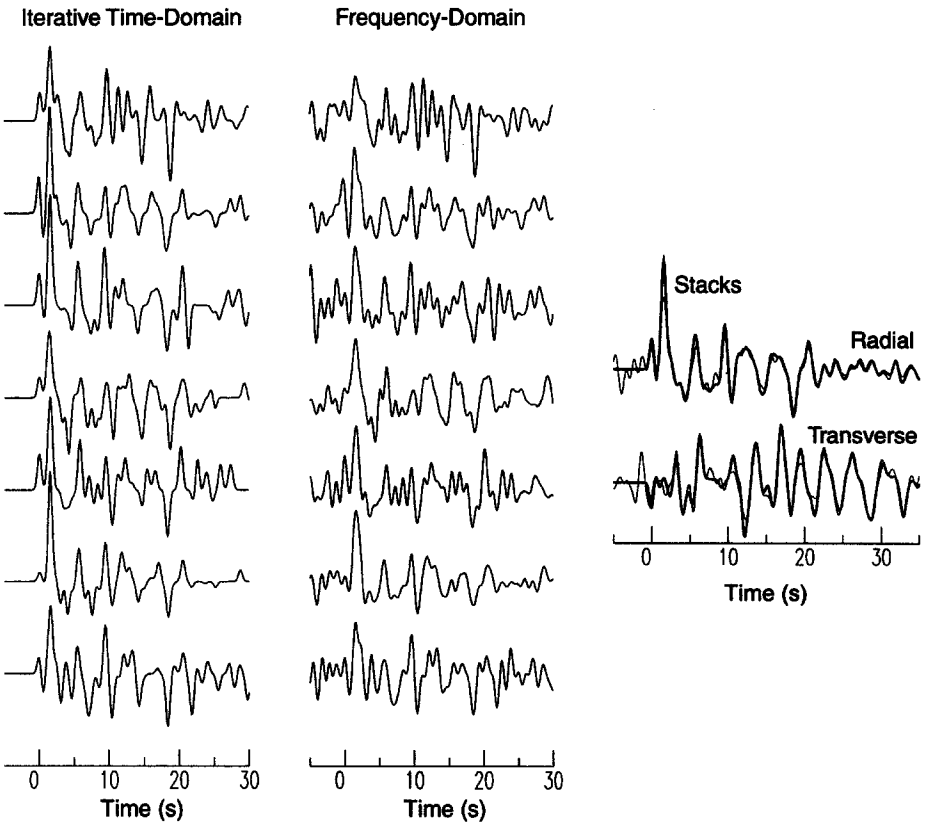

Figure 5. Comparison of receiver-function deconvolutions for events approaching station MLA, located near Long Valley Caldera in eastern California, from the northwest. On the left are the time-domain estimates of the radial receiver function, in the middle are the corresponding water-level frequency-domain receiver functions, and on the right are the average radial and transverse receiver functions from these six events (the thick line identifies the time-domain estimate).

acausal noise on the individual frequency-domain responses. Again, the results are consistent when all the observations are averaged, although the reliability of the *P* arrival might be questioned after examining the noise in the frequency-domain estimates. Once again, the average time-domain variability between the two methods is small, but the amplitude spectra of the iterative time-domain approach are more coherent.

Discussion

The iterative time-domain deconvolution is equally effective for estimating receiver functions using high-quality signals, although it is less efficient than simpler methods such as water-level deconvolution. However, for a modest increase in computation costs, we have a simple, intuitive way of estimating receiver functions that is free of complex relationships between water-level values, time-domain smoothing and damping parameters, and the resulting receiver function. Additionally, the iterative approach has the advantage of *a priori* requiring a level long-period spectrum that helps alleviate acausal troughs in the resulting receiver function, and like other time-domain inversion approaches, the iterative approach easily generalizes to a multi-waveform receiver-function estimation.

Acknowledgments

We thank George Zandt, Susan Beck, George Randall, and Aaron Velasco for their discussions of deconvolution and an anonymous reviewer for helping us to focus and clarify this note. This work was supported by NSF Grant EAR-9628401.

References

Ammon, C. J. (1991). The isolation of receiver effects from teleseismic *P* waveforms, *Bull. Seism. Soc. Am.* **81,** 2504–2510.

Ammon, C. J., G. E. Randall, and G. Zandt (1990). On the nonuniqueness of receiver function inversions, *J. Geophys. Res.* **95,** 15303–15318.

Benz, H. M., R. B. Smith, and W. D. Mooney (1990). Crustal structure of the Northern Basin and Range province from the 1986 Program for Array Seismic Studies of the Continental Lithosphere Seismic Experiment, *J. Geophys. Res.* **95,** 21823–21842.

Cassidy, J. F. (1992). Numerical experiments in broadband receiver function analysis, *Bull. Seism. Soc. Am.* **82,** 1453–1474.

Clayton, R. W., and R. A. Wiggins (1976). Source shape estimation and

deconvolution of teleseismic body waves, *J. R. Astr. Soc.* **47,** 151–177.

Gurrola, H., G. E. Baker, and J. B. Minster (1995). Simultaneous time domain deconvolution with application to the computation of receiver functions, *Geophys. J. Int.* **120,** 537–543.

Julia, J., J. Vila, and R. Macia (1998). The receiver structure beneath the Ebro Basin, Iberian Peninsula, *Bull. Seism. Soc. Am.* **88,** 1538–1547.

Kennett, B. L. N. (1983). *Seismic Wave Propagation in Stratified Media,* Cambridge University Press, New York, 342 pp.

Kikuchi, M., and H. Kanamori (1982). Inversion of complex body waves, *Bull. Seism. Soc. Am.* **72,** 491–506.

Langston, C. A. (1979). Structure under Mount Rainier, Washington, inferred from teleseismic body waves, *J. Geophys. Res.* **84,** 4749–4762.

Mangino, S. G., G. Zandt, and C. J. Ammon (1993). The receiver structure beneath Mina, Nevada, *Bull. Seism. Soc. Am.* **83,** 542–560.

McNamara, D. E., and T. J. Owens (1993). Azimuthal shear wave velocity anisotropy in the Basin and Range province using Moho P_s converted phases, *J. Geophys. Res.* **98,** 12003–12017.

Oldenburg, D. W. (1981). A comprehensive solution to the linear deconvolution problem, *Geophys. J. R. Astr. Soc.* **65,** 331–357.

Owens, T. J. (1984). Determination of crustal and upper mantle structure from analysis of broadband teleseismic P-waveforms, *Ph.D. thesis,* Department of Geology and Geophysics, The University of Utah.

Owens, T. J., and G. E. Randall (1990). The 1988–89 PASSCAL Basin and Range Passive-Source Seismic Experiment. Part I: Large Aperture Array Data, PASSCAL Data Report No. 90-001, Available upon request at the IRIS-Data Management Center.

Peng, X., and E. D. Humphreys (1997). Moho dip and crustal anisotropy in Northwestern Nevada from teleseismic receiver functions, *Bull. Seism. Soc. Am.* **87,** 745–754.

Randall, G. E. (1989). Efficient calculation of differential seismograms for lithospheric receiver functions, *Geophys. J. Int.* **99,** 469–481.

Randall, G. E., and T. J. Owens (1994). Array analysis of the large-aperture array of the 1988–89 PASSCAL Basin and Range passive-source seismic experiment, *Geophys. J. Int.* **116,** 618–636.

Sheehan, A. F., G. A. Abers, A. L. Lerner-Lam, and C. H. Jones (1995). Crustal thickness variations across the Rocky Mountain Front from teleseismic receiver functions, *J. Geophys. Res.* **100,** 20391–20404.

Department of Earth and Atmospheric Sciences
Saint Louis University
3507 Laclede Ave.
St. Louis, Missouri, 63013

Manuscript received 28 August 1998.